

## Reaction and total cross sections for low energy $\pi^+$ and $\pi^-$ on isospin zero nuclei

A. Saunders, S. Hóibråten,\* J. J. Kraushaar, B. J. Kriss, R. J. Peterson, and R. A. Ristinen  
*Nuclear Physics Laboratory, University of Colorado, Boulder, Colorado 80309*

J. T. Brack† and G. Hofman  
*University of British Columbia, TRIUMF, Vancouver, British Columbia, Canada V6T 2A3*

E. F. Gibson  
*California State University, Sacramento, California 95819*

C. L. Morris  
*Los Alamos National Laboratory, Los Alamos, New Mexico 87545*  
 (Received 8 August 1995)

Reaction and total cross sections for  $\pi^+$  and  $\pi^-$  on targets of  $^2\text{H}$ ,  $^6\text{Li}$ , C, Al, Si, S, and Ca have been measured for beam energies from 42 to 65 MeV. The cross sections are proportional to the target mass at 50 MeV, consistent with transparency to these projectiles. The cross sections are compared to theoretical calculations.

PACS number(s): 25.80.Ls

### I. INTRODUCTION

We present a study of 50 MeV  $\pi^+$  and  $\pi^-$  total and reaction cross sections for nuclear targets with equal numbers of protons and neutrons, from deuterium through calcium, in addition to aluminum. We also measured the cross sections for carbon from 42 MeV to 65 MeV. The experiment was designed to minimize the important classes of systematic uncertainties, and many of the necessary corrections were explicitly checked by exaggerating their effects by geometrical changes in the apparatus.

Reaction and total cross sections are valuable observables for a reaction, with sensitivities to the mechanism that may differ from those of elastic scattering, and with an independent set of experimental uncertainties. In terms of the projectile-nucleus non-Coulomb scattering amplitudes,  $\eta_l$ , the cross sections are

$$\sigma_R = \frac{\pi}{k^2} \sum [1 - |\eta_l|^2], \quad (1)$$

$$\sigma_T = \frac{2\pi}{k^2} \sum [1 - \text{Re} \eta_l], \quad (2)$$

where  $k$  is the incoming pion's wave number. The total cross sections are the reaction cross sections plus the elastic scattering due to the nuclear interaction, without the Coulomb amplitudes.

The analysis includes new features to improve the reliability of the results. We used known elastic cross sections in the Monte Carlo modeling for a better representation of the effects of the target. These cross sections were also used to

remove the elastic contributions to the attenuation of the beam in our targets. We used a new method of restoring the nuclear elastic scattering to obtain the total cross sections, using the computed cross sections for neutral pions. The elastic cross sections we used for these features were obtained by fitting known elastic scattering data, and using the parameters so obtained for interpolations to our specific cases.

Since pion-nucleus scattering at low energies has a small cross section, it has long been expected that nuclei will show a transparency to these probes [1]. Indeed, the reaction cross sections of Meirav *et al.* for 50 MeV  $\pi^+$  indicate a constant cross section per target nucleon [2]. This constancy for total cross sections has been taken to indicate a transparency of nuclei to higher energy  $K^+$  mesons [3,4].

At 50 MeV, our results show a close proportionality of  $\pi^+$  cross sections to the target atomic masses above deuterium. The  $\pi^-$  cross sections are not proportional to the target atomic mass; the cross sections divided by the atomic mass increase with atomic mass. The charge-averaged cross section for the two beam polarities (to compensate for Coulomb effects) is about 25 mb per nucleon for total cross sections and about 16 mb for reaction cross sections. Results from the present experiment complement the existing data for total cross sections in the resonance region [5], where a decomposition into the several components has been made [6], by extending the earlier data to much lower energies than previously available. Reaction cross sections from the present work connect the data at 20 and 30 MeV [7] to those near resonance [6].

### II. EXPERIMENTAL METHOD

The reaction and total cross sections were measured using a transmission method [8]. The transmission cross section at any solid angle is

$$\sigma_{\text{TR}} = \sigma_R + \sigma_{\text{EL}} + \sigma_C + \sigma_{\text{NCI}}, \quad (3)$$

\*Present address: FFIWM, N-2007 Kjeller Norway.

†Present address: University of Colorado, Boulder, CO 80309-0446.

where  $\sigma_{\text{TR}}$  is the transmission cross section,  $\sigma_{\text{R}}$  is the reaction cross section,  $\sigma_{\text{EL}}$  is the nuclear elastic cross section,  $\sigma_{\text{C}}$  is the Coulomb cross section, and  $\sigma_{\text{NCI}}$  is the contribution due to nuclear-Coulomb interference. The reaction cross section can be extracted by subtracting the three terms on the right (the “elastic correction”) from the transmission cross section. Finally, the total cross section can be found by adding back the nuclear elastic cross section to the reaction cross section.

The transmission cross section was found by correcting a raw attenuation cross section. The number of pions in the beam was counted, as was the number of pions which did not scatter out of a given solid angle. The beam and unscattered pions were counted with the target both present and removed. The raw attenuation cross section was given by

$$\sigma_{\text{att(raw)}}(\Omega) = \frac{1}{N} \ln \left[ \frac{S_0}{S} \times \frac{B}{B_0} \right], \quad (4)$$

where  $N$  is the areal density of target nuclei,  $B$  is the number of incident beam pions counted with the target present,  $B_0$  is the number counted with the target removed,  $S$  is the number of particles detected by a transmission counter with the target present, and  $S_0$  is the number detected with the target removed. The analysis path which was followed to find the reaction and total cross sections is described in more detail in the next section.

The experiment was conducted using the  $M11$  pion channel at TRIUMF. Both positive and negative pion beams were used, with kinetic energies ranging from 42 MeV to 67 MeV. The channel energy calibration was known to  $\pm 0.25\%$  [9]. The full momentum width of the beam was 0.5% [10]. The channel kinetic energies were offset at each channel setting to account for energy loss in the scintillators and air between the channel exit and the target, to give the target-center energies cited.

The targets used were  $\text{CD}_2$ , C (four thicknesses),  ${}^6\text{Li}$ , Si, S, and Ca. One of the carbon targets was used for the present results, the other three for investigating systematic effects. All the materials were natural except for the separated  ${}^6\text{Li}$  and  $\text{CD}_2$ . The  ${}^6\text{Li}$  target was 95.54% enriched by number, and 99.92% of the target mass was lithium. The hydrogen content of the  $\text{CD}_2$  targets has been measured by neutron capture probabilities, with the impurity determined to be  $2.4 \pm 0.4\%$  [11]. These  $\text{CD}_2$  targets were also used for a  $K^+$  total cross section experiment [3]. An aluminum sample was used to make background subtractions to account for the cladding on the  ${}^6\text{Li}$  and Ca targets. The target thicknesses were chosen so that the beam lost approximately the same energy,  $2.0 \pm 0.2$  MeV, in each target used for the final results. The individual target thicknesses were known to an uncertainty of 3% in the worst case. Target wheels were used to allow rapid target changes. The target centers were at the same position in the  $z$  direction (along the beam axis) to within 1 mm.

The experimental setup is shown in Fig. 1. The counter dimensions are listed in Table I. The beam was defined by four scintillators ( $B1$ – $B4$ ), all of which had to fire for a particle to be counted as a beam particle.  $B1$  was about 1.2 m upstream of the target, and  $B4$  was about 1 cm upstream of the target. This telescope defined a beam spot 2.7 cm in

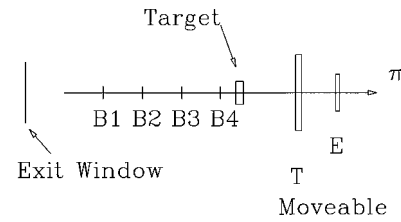


FIG. 1. Diagram of experimental setup, showing channel exit window, beam defining scintillators ( $B1$ – $B4$ ), target, moveable transmission counter ( $T$ ), and moveable efficiency counter ( $E$ ). This figure is not drawn to scale.

diameter with an angular spread of 22 mr. A cut on the relative time of flight between the pion production target and  $B1$  rejected most muons in the beam up to that point. An upper level cut was made on the pulse height in  $B1$  to reject protons in the beam that may have gotten through the channel despite the degrader system at the channel midpoint. Finally, a cut was made on the pulse height in  $B4$  to reject pions which reacted in that detector and deposited a significant amount of energy. The cut on the  $B4$  pulse height allowed this experiment to dispense with a veto counter, unlike some previous experiments [2]. The definition of a beam event was therefore

$$B = (B1 \cdot B2 \cdot B3 \cdot B4) \cdot \text{TOF} \cdot B1\text{PH} \cdot B4\text{PH}. \quad (5)$$

The contamination of the defined beam by other particle species was observed to be less than 1% in our time histograms, consistent with the experience of Ref. [2]. Beam rates were 15 to  $20 \times 10^3$  beam events per second, with systematic checks using rates of  $30 \times 10^3$  and  $7 \times 10^3$  beam events per second. The cyclotron frequency of the TRIUMF proton accelerator was 23.06 MHz, yielding a doubles fraction of  $6 \times 10^{-4}$ .

A scattered event was a beam event which was not detected by the single moveable transmission counter,  $T$ . The transmission counter, which was also used in the experiment of Ref. [2], was circular, with a radius of 10.16 cm. The efficiency of the transmission counter was monitored and found to be stable to one part in  $10^6$  at 99.985% using a smaller scintillator mounted just downstream of the transmission counter. An absorber for produced or recoil protons was mounted in front of the transmission counter during some runs as a systematic check, with no effect on the final cross sections for reasons explained in the next section. The trans-

TABLE I. Dimensions of the six plastic scintillator counters used in this experiment. All the counters were circular, except  $B2$ , which was square. In the radius column, its full edge length is listed. All dimensions are in centimeters.

Counter	Radius (cm)	Thickness (cm)
$B1$	3.02	0.159
$B2$	3.81	0.159
$B3$	1.35	0.159
$B4$	1.29	0.0794
$T$	10.16	0.32
$E$	7.62	0.32

mission and efficiency counters were mounted on a moveable cart so that the solid angle subtended by the transmission counter could be changed. The eight solid angles used ranged from 0.12 sr to 0.96 sr, which corresponded to an angular range of 11.2 degrees to 30.9° relative to the beam axis. The absolute uncertainty in the position of the transmission counter was 0.2 cm, although the position was reproducible between runs (even with different subtended solid angles) to an uncertainty of less than 0.1 cm. The absolute uncertainty in the  $z$  position leads to a two percent uncertainty in the largest subtended solid angle. The solid angles were chosen to be as close as possible to zero in order to improve the accuracy of the extrapolation to find the reaction and total cross sections, as explained in the next section, while still being far enough from zero solid angle to avoid the region where the elastic cross section was very large (less than about 5°). The angular range crosses the muon cone (at about 18°). The effect of pions decaying into muons was accounted for by a time of flight cut (described above) and by the Monte Carlo corrections.

About  $10^7$  beam pions were counted for the cross section measurements at each solid angle, giving a statistical uncertainty of less than 5% for each raw attenuation cross section.

### III. ANALYSIS

The goal of this experiment was to find reaction and total cross sections by measuring attenuation cross sections, then correcting these for known effects to yield the final results. The raw attenuation cross sections were measured over a range of solid angles. They were corrected at each solid angle for Molière multiple scattering and pion decay using Monte Carlo techniques. The integrated computed elastic cross section was then subtracted from the attenuation cross section to find the reaction cross section at each solid angle. Contributions to the cross section from contaminating materials in the targets were subtracted for three of the targets,  $\text{CD}_2$ ,  ${}^6\text{Li}$ , and  $\text{Ca}$ . Finally, the reaction cross sections were extrapolated to zero solid angle to find the actual reaction cross section. To find the total cross section, the computed nuclear elastic cross section was added to the reaction cross section at each angle, and these results were extrapolated to zero solid angle, as suggested in Ref. [12] and described below.

The widely-used GEANT [13] code was used for the Monte Carlo corrections, and was checked against and found to agree with the REVMOC code developed for TRIUMF [14] for one case. The simulation included such experimental details as the different target thicknesses, the different energy loss for full and empty targets, the scintillator dimensions and locations, and the incident beam characteristics. The Monte Carlo corrections were as large as 30% for heavy targets at small angles. The correction for pion decay was kept approximately equal among all the targets by using targets with similar energy losses, thus allowing better comparison between different targets.

Since the GEANT-generated pion-nucleus differential cross sections do not closely match the published data at these low incident pion energies, published elastic differential cross sections [15] were used as input to the code. For scattering angles of less than 5 degrees in the center-of-mass frame,

TABLE II. Second-order optical model parameters in the notation used by the DWPIES code, in units of  $\text{MeV fm}^5$ . (a) lists the parameters at a pion kinetic energy of 50 MeV as a function of target atomic mass  $A$ , while (b) lists the parameters for  $\pi$ -carbon scattering as a function of pion kinetic energy. Previously published elastic differential cross sections were fit by varying these parameters for several cases, and interpolation gave the values listed and used in our analysis. These values do not represent a systematic review of second-order optical model parameters.

(a) Second-order parameters as a function of $A$				
Positive pions				
$A$	$\text{Re } \lambda_s^{(2)}$	$\text{Im } \lambda_s^{(2)}$	$\text{Re } \lambda_p^{(2)}$	$\text{Im } \lambda_p^{(2)}$
6	3.94	6.06	-1.28	-9.71
12	1.22	2.66	-0.544	-3.37
28	0.814	2.90	-0.302	-3.43
32	-0.090	1.81	0.301	-1.90
40	-0.480	0.041	0.785	-0.200
Negative pions				
6	0.200	-1.81	1.12	6.60
12	-0.282	-2.00	2.21	6.84
28	-1.54	-1.85	3.23	7.23
32	-2.03	-1.40	3.46	5.35
40	-2.74	-2.03	6.36	7.34
(b) Second-order parameters as a function of $T_\pi$				
Positive pions on carbon				
$T_\pi(\text{MeV})$	$\text{Re}\lambda_s^{(2)}$	$\text{Im}\lambda_s^{(2)}$	$\text{Re}\lambda_p^{(2)}$	$\text{Im}\lambda_p^{(2)}$
42.0	1.44	3.11	-0.411	-3.66
45.0	1.36	2.94	-0.461	-3.55
46.5	1.32	2.86	-0.486	-3.50
48.0	1.28	2.77	-0.511	-3.44
49.5	1.23	2.69	-0.537	-3.39
50.0	1.22	2.66	-0.544	-3.37
54.0	1.11	2.43	-0.612	-3.23
65.0	0.73	1.69	-0.831	-2.76

where the elastic cross section is dominated by Coulomb scattering, GEANT's calculations were used, but at larger angles separately calculated elastic differential cross sections were substituted. These differential cross sections were calculated using the DWPIES optical model code [16] for all targets except deuterium. To calculate the elastic differential cross section for pion-deuterium scattering, a different code, that of Rockmore and Saghay [17], was used. The geometrical parameters for the optical model code were those of Ref. [18]. The second-order parameters of the optical model were varied to fit the differential cross sections to published pion elastic scattering results [15]. For combinations of energy and target nucleus for which no published elastic scattering data exist, the second-order parameters were interpolated; this interpolation was possible because our fitted second-order parameters varied smoothly with energy and target atomic mass. Interpolation was necessary for some pion energies for pion-carbon scattering, but not for any of the other targets. The second-order parameters used are listed in Table II. While the fitting procedure did not provide a systematic

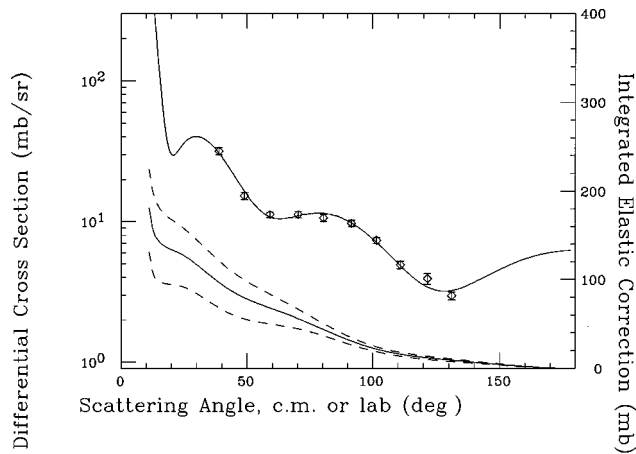


FIG. 2. Fit to the center-of-mass angular distribution of elastic scattering data [15] for 50 MeV  $\pi^+$  on sulfur. The fit used the DWPIES optical model code [16] and allowed the second-order parameters to vary. The lower solid line is the integrated elastic scattering correction. The dashed lines show an error band of the uncertainty in the correction as a function of lab angle, magnified by a factor of 10.

study of optical model parameters, it did provide calculated differential cross sections which matched the published experimental data for our limited number of cases, as shown in Fig. 2, and allowed extrapolation beyond the angular range for which elastic scattering data exist. Since only the few cases needed for this experiment were included in this analysis, this list of second-order parameters is not a replacement for systematic studies such as that of Stricker, McManus, and Carr [19,21]. We only used this means to parametrize the data needed for our analysis.

Application of the Monte Carlo correction to the raw attenuation cross section at each solid angle yielded the attenuation cross section. The integrated elastic cross section, which was subtracted from the attenuation cross section to find the reaction cross section at each solid angle, was found by integrating the output of the optical model code (or Rockmore and Saghai's code for deuterium) from the maximum detector angle to  $180^\circ$ . At the smallest solid angle used in this experiment, with a cone half-angle of  $11.16^\circ$ , the elastic cross section is very steep with angle. Therefore, multiple scattering in the target had an effect on the size of the elastic correction. We accounted for this effect by adjusting the lower limit of the angle integral to include slightly more of the cross section, depending on the amount of multiple scattering in the target. The change in integration limit was as large as  $0.3^\circ$  for silicon and sulfur, our thickest targets, and as small as  $0.02^\circ$  for  $\pi^-$  scattering on  ${}^6\text{Li}$ . The effect on the elastic correction was as large as a 4% increase for sulfur, resulting in a 3% decrease to the reaction cross section at the smallest solid angle. An example of the fitted differential cross section and resulting integral correction is shown in Fig. 2. The elastic cross section used here included the nuclear elastic cross section, the Coulomb cross section, and the cross section caused by nuclear-Coulomb interference.

Three of the targets had significant but known contaminations of other materials whose cross sections had to be subtracted. The deuterium target was in the form of  $\text{CD}_2$ , so the

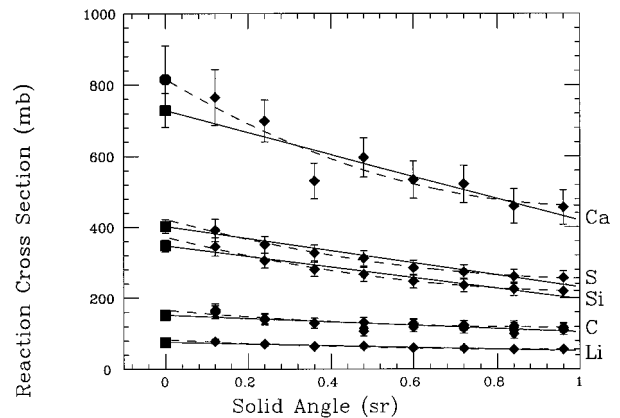


FIG. 3. Examples of linear and quadratic extrapolations to zero solid angle for 50 MeV  $\pi^+$ -nucleus reaction cross sections. The linear fits to the data are shown by solid lines, and the quadratic fits are shown by dashed lines. The linearly extrapolated cross sections are shown by squares. The quadratically extrapolated point is shown for the one case of calcium by a circle, because its error bar did not overlap the linearly extrapolated point. The error bars shown are due to statistics in the experiment and Monte Carlo simulation, as well as uncertainty in the elastic correction, only. The uncertainties due to Monte Carlo statistics and the elastic correction are not completely independent. For  $\pi^+$ -carbon scattering, four independent data sets are shown.

carbon contribution had to be removed. The lithium and calcium targets had aluminum coverings. The reaction cross sections for the contaminants, which were also measured in this experiment, were subtracted at each solid angle for each of the three targets. Finally, the reaction cross sections were extrapolated to zero solid angle to find the actual reaction cross section. Shown in Fig. 3 are linear and quadratic fits to the data for  $\pi^+$ -nucleus scattering. As can be seen in the figure, although the quadratic fits result in extrapolated cross sections that are systematically higher than the linearly extrapolated cross sections, the difference is small, except for calcium. In any case where the two extrapolations did not agree to within their error bars, the linear result was used, but its error bar was increased, to reach the result of the quadratic extrapolation. The extrapolation eliminated any error caused by detection in the transmission counter of recoil protons from back angle pion scattering, because the number of protons detected falls to zero at zero solid angle, and also eliminated any effect of the proton absorbers on the final results, as discussed later.

The total cross sections were found by modifying the technique used to find the reaction cross sections. At each solid angle, the computed nuclear elastic cross section was added to the reaction cross section measured in this experiment. The nuclear elastic cross section was found by integrating the nuclear elastic differential cross section, as was done to find the elastic correction. The nuclear elastic differential cross section was calculated using the optical model code, but with the charge of the pion set to zero to eliminate the Coulomb and nuclear-Coulomb interference parts of the elastic cross section. Since the 50 MeV  $\pi$ -nucleon interaction is weak, this step is very similar to that used to extract  $K^+$ -nucleus total cross sections, based on the weak  $K^+$ -nucleon interaction [12]. The second-order optical model

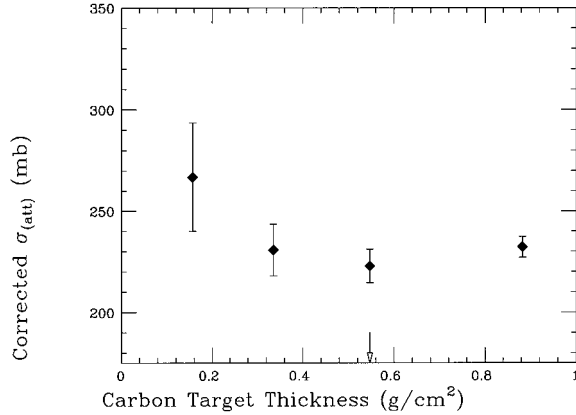


FIG. 4. The 65 MeV  $\pi^+$ -carbon attenuation cross section as a function of target thickness. After being corrected for multiple scattering, pion decay, and other effects, the attenuation cross section is independent of target thickness near the nominal thickness (arrow), used for the final results. These attenuation cross sections were measured at a solid angle of 0.90 sr.

parameters were the same as those used for the full elastic differential cross section measurement, because all the targets had equal numbers of protons and neutrons. The energy of the incident pions was adjusted in the calculation to account for the Coulomb barrier, by changing the pion energy by an amount equal to the surface Coulomb energy caused by a uniformly dense spherical charge  $Z$  with a radius of  $1.2A^{1/3}$  fm. The resulting cross sections were added to the reaction cross sections at each solid angle to yield the total cross section as a function of solid angle. The results were then linearly extrapolated to zero solid angle as for the reaction cross sections (Fig. 3).

Several systematic checks were made. The beam pion rate was varied from 7 to  $30 \times 10^3$  beam pions per second, with an effect on the raw attenuation cross section of less than 2%. Carbon targets of four different thicknesses were used to check the corrections for multiple scattering. The corrected cross sections were independent of target thickness near the nominal thickness (Fig. 4). An absorber in front of the transmission counter was used to absorb recoil protons from back angle pion scattering for some runs. The effect of this absorber was observed to extrapolate to zero at zero solid angle. Two transmission counters in coincidence were used for some runs as well, with the effect of increasing the amount of background signal detected, due to particles scattering in the first transmission counter. Several of the cross section measurements were repeated at widely spaced times in the experiment to ensure repeatability of the measurements. The results of all tests were consistent within their statistical error bars.

#### IV. ERROR ANALYSIS AND RESULTS

The total and reaction cross sections measured in this experiment are summarized in Tables III and IV. The statistical uncertainty of each raw attenuation cross section measurement was less than 5%. The major sources of systematic uncertainty were the correction for elastic scattering, the Monte Carlo correction, the thickness of the targets, and the

TABLE III. Reaction and total cross sections in mb. Reaction and total cross sections for 50 MeV  $\pi$  scattering divided by target atomic mass,  $A$ , as a function of  $A$ . The uncertainties listed in parentheses include all statistical and systematic uncertainties.

Target	$A$	Positive pions		Negative pions	
		$\sigma_R/A$	$\sigma_T/A$	$\sigma_R/A$	$\sigma_T/A$
$^2\text{H}$	2	10.0(1.8)		12.2(1.9)	
$^6\text{Li}$	6	12.7(1.4)	19.5(1.9)	16.7(2.0)	22.3(2.3)
C	12	12.7(1.2)	20.6(1.7)	14.8(2.0)	23.8(2.6)
Al	27	13.3(1.3)	22.1(2.0)	20.4(2.2)	29.8(2.8)
Si	28	12.4(1.2)	21.5(1.9)	21.1(2.3)	30.5(2.9)
S	32	12.6(1.2)	21.4(1.9)	21.6(2.4)	31.1(3.0)
Ca	40	18.2(2.1)	27.7(2.7)	24.2(3.2)	34.9(3.8)

uncertainty in the solid angle subtended by the transmission counter.

The systematic uncertainties on each solid angle measurement caused by the elastic correction were estimated to be between one and four percent, depending on the target. These uncertainties were estimated by assuming that the primary sources of uncertainty were the second-order parameters used in the optical model code. As described in Sec. III, these parameters were found by fitting the elastic scattering differential cross sections to the published data, and therefore had associated error bars based on the uncertainties in the data set and the quality of the fit. To estimate the uncertainty in the integrated elastic correction, the optical model calculation was repeated with the second-order parameters varied within their error bars. The uncertainty assigned to the correction was the maximum change that developed. An example of the uncertainty in the elastic correction (magnified by a factor of 10 for clarity) is shown by error bands on the correction in Fig. 2. A greater quantity of published data for pion elastic scattering on a given target nucleus resulted in better determined second-order parameters, and hence a better determined elastic scattering correction for that target. The best determination, with an uncertainty of one percent, was for a carbon target with 50 MeV pions, and the worst, with uncertainties as large as 4%, were for the cases where interpolation of the second-order parameters was necessary.

The elastic scattering data had uncertainties in their angular distribution, as discussed above, but also had overall nor-

TABLE IV. Reaction and total cross sections in mb. Reaction and total cross sections for  $\pi^+$ -carbon scattering as a function of pion kinetic energy. The uncertainties listed in parentheses include all statistical and systematic uncertainties.

$T_\pi$ (MeV)	$\sigma_R$	$\sigma_T$
42.0	125(14)	214(18)
45.0	135(15)	228(19)
46.5	137(14)	232(19)
48.0	140(20)	238(27)
49.5	158(19)	259(25)
50.0	152(14)	248(20)
54.0	147(14)	253(20)
65.0	202(17)	329(24)

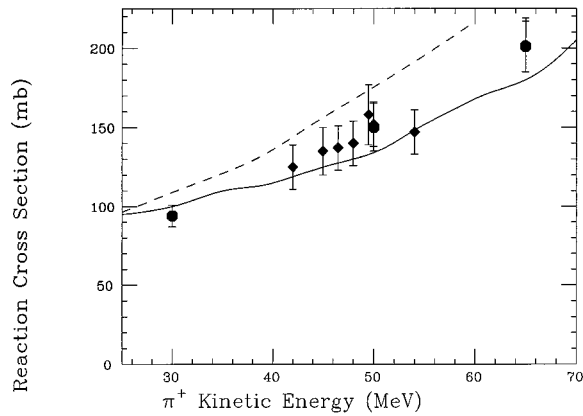


FIG. 5. Carbon reaction cross sections as a function of  $\pi^+$  kinetic energy. The diamonds are the results of the present experiment. The circles are the previous results of Meirav *et al.* [2]. The solid line is the calculation by Khankhaseyev [24]. The dashed line is an optical model calculation by Nieves, Oset, and Garcia-Recio [23]. The error bars on the present results are due to all systematic and statistical uncertainties.

malization and systematic uncertainties, which were not reflected in our fitting procedure. The quoted overall uncertainties in the elastic scattering database [15] ranged from 4% to 15%, depending on the means used to normalize the elastic data. These uncertainties were included in the uncertainty applied to each elastic correction. Although the above uncertainties apply to the elastic correction, the uncertainties of the final cross sections are of similar magnitude, since the elastic correction was of about the same size as the final cross section in most cases. In the case of positive pion scattering on carbon, the effect of a 10% uncertainty in the elastic correction was a contribution of 4.5% to the uncertainty of the reaction cross section, while for positive pion scattering on calcium the effect of a 15% uncertainty was a contribution of 9%. The elastic scattering correction was the largest source of uncertainty in this experiment.

The second major source of uncertainty was the Monte Carlo correction. This source of error had two parts: first, the statistical uncertainty due to the limited number of particles thrown in the Monte Carlo simulations, and second, the systematic errors in the simulation. The statistical uncertainty was held to about 5% of the Monte Carlo correction for all cases. The systematic errors were estimated to be less than 10% of the correction, based on knowledge of the target thicknesses and compositions and replacement of GEANT's internal differential cross sections with externally calculated cross sections. The Monte Carlo corrections were 10 to 30% of the final cross sections, so the uncertainties caused by the corrections were about 1 to 3%.

The uncertainty in the target thickness was about 3% in the worst case. The systematic uncertainties in the final results caused by the uncertainty in the solid angle subtended by the transmission counter were calculated to be less than 1%, based on an uncertainty of 0.2 cm in the location of the transmission counter relative to the target.

The error bars shown in Figs. 5–8 and the values listed in Tables III and IV include all the statistical and systematic uncertainties listed above. The systematic uncertainties did not exceed 15%.

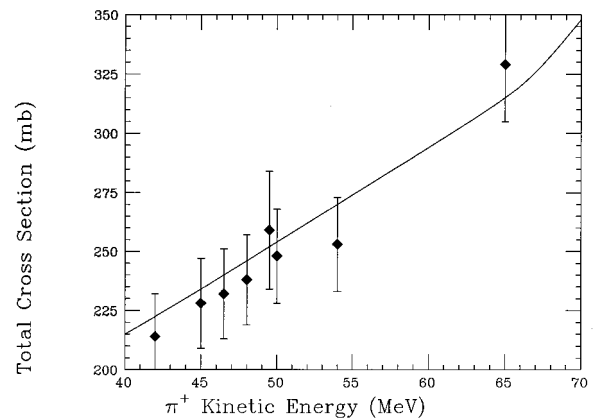


FIG. 6. Carbon total cross sections as a function of  $\pi^+$  kinetic energy. The diamonds are the results of the present experiment. The solid line is the calculation by Khankhaseyev [24]. The error bars on the present results are due to all statistical and systematic uncertainties.

## V. COMPARISONS AND DISCUSSION

Reaction cross section data from a similar transmission experiment carried out by Meirav *et al.* [2] are compared to the present work for the mass dependence at 50 MeV in Fig. 7. Many features of the experiments were very similar, but certain improvements in the analysis were followed in the new work. Reaction cross sections are in very close agreement for the targets common to both experiments, except for  $^{40}\text{Ca}$ . For that case our value is significantly above that of Meirav *et al.*, and a different trend with increasing target mass would be inferred from the two data sets. The beam energy dependences of the carbon  $\pi^+$  reaction cross sections from the two experiments are compared in Fig. 5, with fair agreement.

The target mass dependence of the cross sections, shown in Figs. 7 and 8, results in part from a Coulomb effect. The

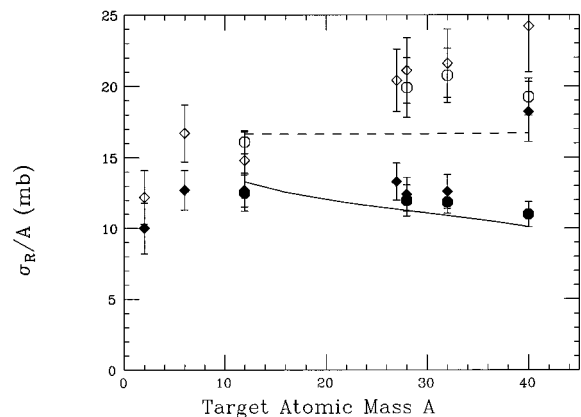


FIG. 7. Reaction cross sections per nucleon, as a function of target atomic mass. The incident pion energy was 50 MeV. The diamonds are the results of the present experiment. The circles are the previous results of Meirav *et al.* [2]. The open symbols are the  $\pi^-$  results, while the solid symbols are the  $\pi^+$  results. The error bars on the present results are due to all systematic and statistical uncertainties. The dashed line is an optical model prediction of the  $\pi^-$  results, while the solid line is a prediction of the  $\pi^+$  results [21].

$\pi^-$  are attracted toward larger  $Z$  nuclei, and scatter at an energy nearer the large  $\Delta$  resonance maximum. The  $\pi^+$ , in contrast, are repelled by the larger  $Z$  nuclei, and scatter at an energy farther from the resonance. We have estimated the size of this effect using a Coulomb offset energy due to a uniform nuclear radius of  $1.2A^{1/3}$  fm, evaluating the pion-proton average of both signs using total cross sections from a recent phase-shift compilation [20]. Relative to  ${}^6\text{Li}$ , the  $\pi^-$  cross sections on calcium should increase by 16%, while the  $\pi^+$  cross sections should decrease by 13%. The cross sections in Figs. 7 and 8 increase by more than expected from this effect.

Optical model calculations of reaction and total cross sections have been reported, sometimes without data for comparison. In Figs. 7 and 8, we show curves connecting these optical model results for 50 MeV pions on targets of  ${}^{12}\text{C}$ ,  ${}^{16}\text{O}$ , and  ${}^{40}\text{Ca}$ , using a second-order potential with parameters determined by systematic fits to elastic scattering [21]. This work provides a more reliable set of second-order parameters than was obtained for our work. The trend of the  $\pi^+$  reaction cross sections is to decrease somewhat more rapidly with target mass than do our results. The predicted  $\pi^-$  reaction cross sections generally lie below those we observe. For both charge states, agreement is found for  ${}^{12}\text{C}$ , where the elastic scattering data base is most secure. Computed total cross sections for both signs are significantly below most of our observations, as seen in Fig. 8, with near agreement again found near  ${}^{12}\text{C}$ . Another comparison is possible for the case of  ${}^{27}\text{Al}$ , where 50 MeV reaction cross sections are computed to be 263 mb ( $\pi^+$ ) and 414 mb ( $\pi^-$ ) using parameter set  $E$  [19]. Our determinations for  ${}^{27}\text{Al}$  are  $359 \pm 19$  mb for  $\pi^+$  and  $597 \pm 19$  mb for  $\pi^-$ . Carr, McManus, and Stricker-Bauer [19] compared computed and measured [22] absorption cross sections for  ${}^{27}\text{Al}$ , but reaction cross section data were not available. Absorption is the part of the reaction cross section in which no pion is present in the final state. Computed absorption cross sections [19] were below the measured values [22], but the differences of  $52 \pm 15$  and  $36 \pm 20$  mb are not enough to account for the difference between computed and our measured reaction cross sections. Overall, the computed values for both  $\pi^+$  and  $\pi^-$ , for both absorption and reaction cross sections, are in the same ratio to our results and those of Nakai *et al.* [22]. In Fig. 5, we show a curve from the optical model calculation of Nieves, Oset, and Garcia-Recio [23]. Their curve lies significantly above our values at all energies, and also above all the data points reported by Meirav *et al.* in our energy range.

We also compare the energy dependence of our data to results from the unitary scattering theory [24], using an average excitation energy parameter  $\Delta$  of 20 MeV. Comparisons are shown in Figs. 5 and 6. Computed reaction cross sections are above the data for energies below 60 MeV and below the data above this energy. Computed total cross sections are also above the measured values below 60 MeV. Changes in the parameter  $\Delta$  have been shown to enable the theory to account for these effects [24].

Also shown in Fig. 8 are the total cross sections per target nucleon for a  $K^+$  beam of 531 MeV/c [3]. This projectile has been important for studies of nucleons within nuclei because of its long mean free path. The present data for 50 MeV  $\pi^+$  show somewhat larger total cross sections than do the

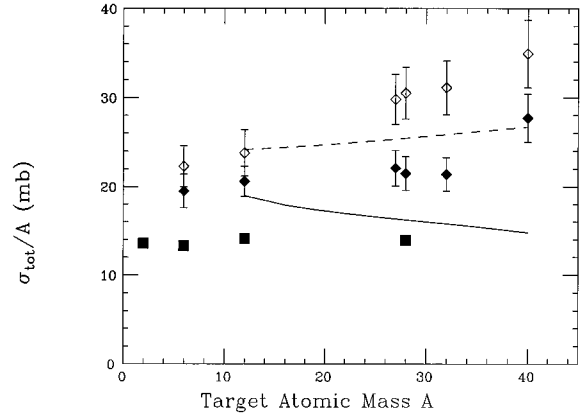


FIG. 8. Total cross sections per nucleon, as a function of target atomic mass. The incident pion kinetic energy was 50 MeV. The diamonds are the results of the present experiment. The solid diamonds are the  $\pi^+$  results, and the open diamonds are the  $\pi^-$  results. The solid squares are the  $K^+$  results at 531 MeV/c measured by Weiss *et al.* [3]. The error bars on the  $K^+$  results are smaller than the symbols. The error bars on the present results are due to all systematic and statistical uncertainties. The dashed line is an optical model prediction of the  $\pi^-$  cross sections, while the solid line is a prediction of the  $\pi^+$  cross sections [21].

$K^+$  data, and an equally uniform cross section, which shows evidence for nuclear transparency. It must be emphasized, however, that the wavelength of the 50 MeV  $\pi^+$  is much greater than that of the internucleon spacing, and that therefore the present experiment did not sense individual nucleons within the nucleus.

Partial total cross sections for the disappearance of 50 MeV  $\pi^+$  on carbon and deuterium have been reported [25]. That experiment found a ratio of 10.3 for these cross sections, compared to a value of six incoherent deuterons that might be expected in carbon. We observe a ratio of reaction cross sections of  $7.5 \pm 0.6$ , perhaps indicating a smaller relative effect of coherent reaction mechanisms than found in the partial total cross sections.

In conclusion, we have measured total and reaction cross sections for 50 MeV positive and negative pions on a range of nuclei with zero isospin and for 42 to 65 MeV pions on carbon. The positive pion cross sections are nearly proportional to the target mass number for nuclei heavier than deuterium, and the negative pion cross sections have a higher than linear dependence on the target mass number. The present results form a consistent study of pion-nucleus total and reaction cross sections in this energy and target mass range because of the control of the sources of error maintained during the experiment. They provide constraints on optical model analyses of pion scattering, and complement the previously existing data set.

#### ACKNOWLEDGMENTS

We wish to acknowledge the support of the TRIUMF technical and support staff and to thank D. Ottewell, G. R. Smith, and M. Pavan. Financial support has been provided in part by the U.S. Department of Energy (Grant No. DE-FG03-95ER-40913). TRIUMF is supported in part by the Natural Sciences and Engineering Research Council of Canada.

- [1] W. R. Gibbs, W. B. Kaufmann, and J.-P. DeDonder, *Phys. Lett. B* **231**, 6 (1989).
- [2] O. Meirav, E. Friedman, A. Altman, M. Hanna, R. R. Johnson, and D. R. Gill, *Phys. Rev. C* **36**, 1066 (1987); O. Meirav, E. Friedman, R. R. Johnson, R. Olszewski, and P. Weber, *ibid.* **40**, 843 (1989).
- [3] R. J. Weiss *et al.*, *Phys. Rev. C* **49**, 2569 (1994).
- [4] R. A. Krauss *et al.*, *Phys. Rev. C* **46**, 655 (1992).
- [5] A. S. Carroll, I-H. Chiang, C. B. Dover, T. F. Kycia, K. K. Li, P. O. Mazur, D. N. Michael, P. M. Mockett, D. C. Rahm, and R. Rubinstein, *Phys. Rev. C* **14**, 635 (1976).
- [6] D. Ashery, I. Navon, G. Azuelos, H. K. Walter, H. J. Pfeiffer, and F. W. Schlepütz, *Phys. Rev. C* **23**, 2173 (1981).
- [7] E. Friedman, A. Goldring, R. R. Johnson, O. Meirav, D. Vetterli, P. Weber, and A. Altman, *Phys. Lett. B* **257**, 17 (1991).
- [8] G. Giacomelli, *Progress in Nuclear Physics* (Pergamon Press, Oxford, 1970), Vol. 12, part 2.
- [9] M. Pavan (private communication).
- [10] TRIUMF Users Group Executive Committee, *TRIUMF User's Handbook* (Rev. 1987).
- [11] R. E. Chrien (private communication).
- [12] W. B. Kaufmann and W. R. Gibbs, *Phys. Rev. C* **40**, 1279 (1989).
- [13] GEANT Version 3.15, Data Handling Division, CERN DD/EE/84-1.
- [14] P. Kitching, TRIUMF publication, TRI-71-2 (1971).
- [15] S. A. Dytman *et al.*, *Phys. Rev. C* **18**, 2316 (1978); M. A. Moinester *et al.*, *ibid.* **18**, 2678 (1978); R. R. Johnson, T. G. Masterson, K. L. Erdman, A. W. Thomas, and R. H. Landau, *Nucl. Phys.* **A296**, 444 (1978); M. Blecher *et al.*, *Phys. Rev. C* **20**, 1884 (1979); B. M. Preedom *et al.*, *ibid.* **23**, 1134 (1981); S. H. Dam *et al.*, *Phys. Rev. C* **25**, 2574 (1982); M. Blecher *et al.*, *ibid.* **28**, 2033 (1983); R. J. Sobie *et al.*, *ibid.* **30**, 1612 (1984); U. Wienands *et al.*, *ibid.* **35**, 708 (1987); K. K. Seth *et al.*, *ibid.* **41**, 2800 (1990); G. Burleson *et al.*, *ibid.* **49**, 2226 (1994).
- [16] R. A. Eisenstein and G. A. Miller, *Comput. Phys. Commun.* **11**, 95 (1976); M. B. Johnson, *Phys. Rev. C* **22**, 192 (1980); M. B. Johnson and E. R. Siciliano, *ibid.* **27**, 1647 (1983).
- [17] R. Rockmore and B. Saghai, *Phys. Rev. C* **28**, 2064 (1983).
- [18] H. de Vries, C. W. de Jager, and C. de Vries, *At. Data Nucl. Data Tables* **36**, 495 (1987).
- [19] J. A. Carr, H. McManus, and K. Stricker-Bauer, *Phys. Rev. C* **25**, 952 (1982).
- [20] R. A. Arndt, J. M. Ford, and L. D. Roper, *Phys. Rev. D* **32**, 1085 (1985).
- [21] K. Stricker, H. McManus, and J. A. Carr, *Phys. Rev. C* **19**, 929 (1979).
- [22] K. Nakai, T. Kobayashi, T. Numao, T. A. Shibata, J. Chiba, and K. Masutani, *Phys. Rev. Lett.* **44**, 1446 (1980).
- [23] J. Nieves, E. Oset, and C. Garcia-Recio, *Nucl. Phys.* **A554**, 554 (1993).
- [24] M. K. Khankhasayev, *Nucl. Phys.* **A505**, 717 (1989).
- [25] M. W. Rawool-Sullivan, C. L. Morris, J. M. O'Donnell, M. K. Jones, K. O. Oganesyan, E. A. Paseuk, A. I. Reshetin, F. F. Guber, and B. Ritchie, *Bull. Am. Phys. Soc.* **38**, 943 (1993).